sciendo

LATVIAN JOURNAL OF PHYSICS
AND TECHNICAL SCIENCES
2023, N 6

DOI: 10.2478/lpts-2023-0037

NON-ENZYMATIC Co_3O_4 NANOSTRUCTURE-BASED ELECTROCHEMICAL SENSOR FOR H_2O_2 DETECTION

V. Mizers[1*], V. Gerbreders[1], M. Krasovska[1], E. Sledevskis[1],
I. Mihailova[1], A. Ogurcovs[1,2], A. Bulanovs[1], A. Gerbreders[2]

[1] G. Liberts' Innovative Microscopy Centre, Department of Technology,
Institute of Life Sciences and Technology, Daugavpils University,
1a Parades Str., Daugavpils, LV-5401, LATVIA
[2] Institute of Solid State Physics, University of Latvia,
8 Kengaraga Str., Riga, LV-1063, LATVIA
*e-mail: valdis.mizers@du.lv

This article describes the synthesis of nanostructured cobalt oxide on iron wires and its application for the detection of hydrogen peroxide as working electrode for non-enzymatic electrochemical sensor. Cobalt oxide was obtained by the hydrothermal synthesis method using chloride and acetate anions. The resulting nanostructured coating obtained from the chloride precursor is a uniform homogeneous porous network of long nanofibers assembled into regular honeycomb-like formations. In the case of an acetate precursor, instead of nanofibers, petal-like nanostructures assembled into honeycomb agglomerates are observed. The structure, surface, and composition of the obtained samples were studied using field-emission scanning electron microscopy along with energy-dispersive spectroscopy and X-ray diffractometry.

The resultant nanostructured specimens were utilized to detect H_2O_2 electrochemically through cyclic voltammetry, differential pulse voltammetry, and i-t measurements. A comparative research has demonstrated that the nanostructures produced from the chloride precursor exhibit greater sensitivity to H_2O_2 and have a more appropriate morphology for designing a nanostructured sensor. A substantial linear correlation between the peak current and H_2O_2 concentration within the 20 to 1300 μM range was established. The Co_3O_4 electrode obtained exhibits a sensitivity of 505.11 $\mu A \cdot mM^{-1}$, and the electroactive surface area is calculated to be 4.684 cm^2. Assuming a signal-to-noise ratio of 3, the calculated limit of detection is 1.05 μM. According to the interference study, the prevalent interfering agents, such as ascorbic acid, uric acid, NaCl, and glucose, do not influence the electrochemical reaction. The obtained results confirm that this sensor is suitable for working with complex analytes.The actual sample assessment demonstrated a recovery rate exceeding 95 %.

Keywords: *Electrochemical sensor, cobalt oxide, cyclic voltammetry, hydrogen peroxide, nanostructures.*

1. INTRODUCTION

Hydrogen peroxide is a strong oxidant and has found wide application in chemical industry, paper production, medicine and food industry. [1] Since hydrogen peroxide is considered relatively safe for humans [2]–[5] it has found wide application as a bleaching and disinfecting agent in various household chemicals, cosmetics and medical products. In a number of countries, hydrogen peroxide is used for water treatment [6]–[8] and preservation of food products (for example, milk) [9], [10].

In living organisms, hydrogen peroxide is formed as a result of incomplete reduction of oxygen during metabolism and is one of the most important reactive oxygen species, which are a by-product of many physiological and pathophysiological processes, such as metabolism, iron proliferation and homeostasis, antioxidant and anti-inflammatory response, response to DNA damage and many others. That is why various reactive oxygen species (and H_2O_2, in particular) are always present in living organisms in small concentrations [11].

However, when the antioxidant defense of the body fails and the concentration of reactive oxygen species exceeds natural values, an oxidative stress occurs. Oxidative stress leads to a damage of nucleic acids, proteins and lipids, which is the cause of various pathological conditions, such as accelerated aging of the body, neurodegeneration, and can also provoke the development of serious diseases such as atherosclerosis and diabetes [12]–[16].

An increase in the concentration of hydrogen peroxide can also be associated with cancer: it has been proven that malignant tumor cells contain up to 100 μM H_2O_2, while the concentration of H_2O_2 in normal cells usually does not exceed 20 nM [17]–[20]. For some types of cancer, such as lung cancer, an increase in the concentration of H_2O_2 in the exhalation is characteristic [18], as well as an increase in the concentration in the blood [21]–[23]. That is why the determination of the concentration of hydrogen peroxide in the blood and other biological fluids can serve as an additional method for diagnosing these diseases [24]–[26].

In various publications, the concentration of H_2O_2 in the blood plasma of a healthy person is indicated in a very wide range from 1 μM to 40 μM. The indicated maximum, although not fatal, is quite stressful and destructive for the cells. Probably, overestimated concentration values were obtained as a result of the peculiarities of the measurement protocol and under the influence of interfering substances that contribute to the obtained value. Since the level of hydrogen peroxide in living organisms is maintained by regulatory mechanisms, and in particular by peroxidase and catalase, the most probable concentration of peroxide in the blood of a healthy individual is in the range of 1–5 μM. However, the possibility of an increase in the concentration of hydrogen peroxide due to the presence of the aforementioned diseases should not be ruled out. Therefore, during the experiment it is very important to carefully study the influence of other substances on the accuracy of the measurement in order to exclude the possibility of the

influence of interferents and to distinguish a false increase in concentration due to the influence of foreign substances from an increase caused by a disease. In addition to medicine, rapid and accurate determination and control of the H_2O_2 concentration is an important task in many other areas, including pharmaceuticals [27], [28], food production [29]–[32], and environmental protection [33].

A number of conventional methods used for concentration measurements for various chemicals (such as titration [34], [35], chemiluminescence [36], [37], and spectrophotometry [38]–[40]) are not suitable for H_2O_2 determination. These methods have a list of disadvantages such as the need for complex equipment (as a result, the need to transport the sample to the laboratory), low sensitivity, significant measurement time, and the need for manual sample preparation. These factors can significantly affect the measurement accuracy due to degradation of samples and changes in the concentration of hydrogen peroxide due to its natural decomposition in the process of sample storage and preparation.

Therefore, at present, the method of electrochemical detection has become widespread [41]–[44]. This method is simple, fast, and accurate. The selectivity of this method allows to avoid a false increase in concentration and eliminating the influence of interfering substances [45], [46]. Based on this method, it has already become possible to create portable devices that allow measurements to be taken directly at the place of sampling without transportation. This can be relevant both in the field of medicine and in the field of environmental monitoring, in particular for monitoring the quality of wastewater.

Electrochemical measurements use working electrodes that can either be modified or unmodified. Modified electrodes are functionalized with redox-active enzymes to ensure accurate and selective measurements, such as the widely used horseradish peroxidase for detecting hydrogen peroxide [47]–[50]. However, using enzymes comes with significant drawbacks, such as increased production costs and reduced electrode stability due to their vulnerability to thermal and chemical damage. To overcome these drawbacks, non-enzymatic electrochemical sensors are becoming more popular, where H_2O_2 interacts directly with the electrode material, resulting in catalytic processes that produce an unambiguous electrochemical response [51]–[54].

Carbon materials [20], as well as thin films of metals [55], [56], and metal oxides [57], [58] are widely used as sensor materials. Utilizing these substances in the nanopowder and nanostructure configuration enables a substantial enhancement in sensor sensitivity by multiplying the active surface area of the functioning electrode[59].

Among the nanostructured materials used, cobalt oxide (Co_3O_4) is a promising candidate [60], [61].

Cobalt oxide is widely employed in supercapacitors and sensors for various applications, including glucose and hydrogen peroxide sensors. It exhibits diverse morphologies such as nanocubes, nanoplates, and nanowhiskers, which can be controlled by altering the precursor ions during hydrothermal synthesis (commonly chloride, nitrate, acetate, and cobalt sulfate) and incorporating structure-directing agents like ammonia, ethanol, and alkali solutions.

A commonly used method to apply

Co_3O_4 nanostructures onto electrodes involves obtaining them as a powder [62], followed by dipping or drop coating techniques with a porous substrate [63] or binder polymers [64]. However, this approach has drawbacks, such as uneven suspension distribution leading to variations in electrochemical properties, repeatability issues, poor adhesion, and low mechanical stability of the coating. These challenges can be overcome by utilizing a hydrothermal growth process, enabling the epitaxial growth of well-ordered nanostructured layers directly onto the wire electrode substrate, facilitated by specific anions or additives.

This technique results in the formation of nanostructures with a significant active surface area, facilitating an efficient electron charge transfer between Co_3O_4 nanostructures and the substrate due to high-density honeycomb-like nanostructured aggregates.

This article focuses on the preparation of nanostructured Co_3O_4 electrodes using the hydrothermal method and demonstrates the exceptional selectivity and sensitivity of the resulting wire electrodes in electrochemically detecting H_2O_2. The study also investigates the influence of precursor anions on the nanostructure's morphology and, consequently, the sensor's sensitivity. Essential electrochemical measurements have been performed to determine H_2O_2 concentrations in aqueous solutions using the developed sensor, and experiments have been conducted to detect H_2O_2 in real samples of UHT milk and contact lens storage liquid.

2. MATERIALS AND METHODS

2.1 Materials

Merck was the source of Cobalt(II) chloride hexahydrate (CAS number: 7791-13-1), cobalt(II) acetate tetrahydrate (CAS number: 6147-53-1), hexamethylenetetramine CH_4N_2O (CAS number: 100-97-0), sodium hydroxide (NaOH, CAS number: 1310-73-2), and 30% hydrogen peroxide solution (H_2O_2, CAS number: 7722-84-1). The reagents were of at least 99.8% purity. Ascorbic acid ($C6H_8O_6$, CAS number: 50-81-7), uric acid ($C_5H_4N_4O_3$, CAS number: 69-93-2), glucose ($C_6H_{12}O_6$, CAS number: 50-99-7), and sodium chloride (NaCl, CAS number: 7647-14-5) were procured from Sigma Aldrich and were also of at least 99.8% purity. The laboratory obtained distilled water. Iron wire (99.9% purity, 2 mm thickness) and Ag/AgCl wire were procured from Sigma Aldrich and A-M Systems, USA, respectively. Additionally, carbon rods (5 mm diameter) were purchased from Sigma Aldrich.

2.2 Co_3O_4 Layer Synthesis on Iron Wire

Iron wire was used as a base to obtain the nanostructured layer. Prior to the synthesis of the nanostructured coating, the wire was treated with fine sandpaper and immersed in 0.1 M HCl to increase the roughness of electrode surface and improve the adhesion of the nanostructures. An equimolar aqueous solution of 0.1 M $CoCl_2*6H_2O$ and CH_4N_2O was mixed in 80 mL distilled water to form

a red violet growth solution. The solution was stirred until the solid reagents dissolved completely and then moved with the pretreated iron wire together into a 100 mL glass beaker covered with a glass lid in the preheated oven. The growth took place at 5 h and 95 ºC, resulting in a dull pink $Co(OH)_2$ coating on the wire. Once cooled to room temperature, the substrate was rinsed with deionized water multiple times to eliminate any leftover reagents and subsequently dried at 80ºC overnight. The growth process was followed by thermal decomposition of $Co(OH)_2$ for 1 h at 450 ºC to obtain Co_3O_4. After annealing, a black, homogeneous Co_3O_4 coating was observed on the wire surface.

To investigate how the acetate anion affects the morphology of Co_3O_4 nanostructures, 0.1 M $(CH_3COO)_2Co*4H_2O$ was used. The rest of the synthesis process took place under the same parameters as in the case with the use of cobalt chloride.

The surface morphology of the nanostructured Co_3O_4 samples was examined using field-emission scanning electron microscopy (FESEM, Tescan MAIA 3), while energy-dispersive spectroscopy (EDS, Inca Synergy) was used to determine their chemical composition. The crystalline structure of the samples was determined using an X-ray diffractometer (RIGAKU Smart Lab, Cu Kα [λ = 1.543 Å]), which employed a parallel beam scanning geometry and an additional Ge(220) × 2 bounce monochromator.

3. ELECTROCHEMICAL MEASUREMENTS

To ensure an improved electrical contact with the equipment, wire samples coated with nanostructures were cut into 3 cm long pieces, and the end of one side was stripped to expose pure iron over a length of 1 cm. The measurements were conducted using an electrochemical station (Zanher, Germany), employing a three-electrode cell setup. The cobalt oxide-coated iron wire served as the working electrode, a 2 mm diameter Ag/AgCl wire acted as the reference electrode, and a 5 mm diameter carbon rod functioned as the counter electrode. Cyclic voltammetry (CV) was performed within the range of -1.3 V to 0.5 V vs Ag/AgCl, with an initial potential of 0 V and a scan rate of 100 $mV \cdot s^{-1}$. A buffer solution of 0.1 M NaOH was utilized. For the detection of H_2O_2, concentrations ranging from 0.2 mM to 5 mM were employed, including 0.2, 0.4, 0.6, 0.8, 1, 2, 3, 4, and 5 mM. Each concentration was tested five times, and the resulting graphs in subsequent sections represent the averaged data from all measurements. The relationship between the electrochemical current response and solution pH and scanning speed was analysed to achieve maximum sensitivity of the sensor. Impedance spectroscopy was performed across a frequency range of 1 Hz to 100 kHz, with an applied signal voltage of approximately 0.25 V. To investigate the current response, a fixed voltage of U = -1.23 V vs Ag/AgCl was applied to the cell, and the resulting current was measured. A buffer solution of 0.1 M NaOH was used for the experiment. Initially, the measurement was conducted in a buffer solution without hydrogen peroxide, allowing for a stabilization period of 120 s. Subsequently, 20 µM portions of H_2O_2 were added at intervals of 120 s. The concentration of H_2O_2 ranged

from 20 μM to 1300 μM, with increments of 20 μM in the range of 0–200 μM, 50 μM in the range of 250–700 μM, and 100 μM in the range of 800–1300 μM. The measurement was carried out with continuous stirring using a magnetic stirrer.

To examine the interference of commonly encountered substances, a constant voltage of U = -1.23 V vs Ag/AgCl was applied to the cell, and the resulting current was measured. A buffer solution of 0.1 M NaOH was used for the experiment. The measurement began with a pure buffer solution (0 μM H_2O_2), and every minute, H_2O_2 or an interferent was added to the solution at a concentration of 100 μM. The substances were added in the following order: H_2O_2, ascorbic acid, uric acid, glucose, and NaCl. This cycle was repeated three times, and the measurement was conducted with continuous stirring using a magnetic stirrer. To demonstrate the practical application potential of Co_3O_4 nanostructured electrodes in electrochemical sensor development, ultra-high temperature processed (UHT) milk and contact lens storage solution were investigated. These substances have complex compositions and were chosen to assess the impact of the sample matrix on the sensor's accuracy. Milk with 3.2% fat content was purchased from a local supermarket, and contact lens storage solution (Diviniti Ocean Moist multi-purpose contact lens care solution) was obtained from a local optical salon. To minimize the influence of the sample matrix, the milk and lens storage solution was diluted in a 1:2 ratio with a standard 0.1 M NaOH buffer solution. The amperometric response method was employed for the analysis, with U = -1.23 V vs Ag/AgCl.

4. RESULTS AND DISCUSSION

As a result of the hydrothermal synthesis, a homogeneous black coating with good adhesion to the surface has been obtained. High mechanical resistance allows for the pretreatment of samples necessary for the electrochemical measurements to be carried out and storage without loss of their quality.

SEM images of the Co_3O_4 nanostructures with nanoporous morphology obtained from the precursor of cobalt chloride and urea are shown in Fig. 1(a–b). The surface of the wire is covered with a homogeneous porous network of long nanofibers assembled into regular honeycomb-like formations.

The acetate anion has effectively changed the morphology of the Co_3O_4 nanostructures. A network of honeycomb formations is still observed on the surface; however, instead of nanostructured fibers, they consist of very thin petal-like structures. In addition, the honeycombs themselves are much smaller in size compared to the chloride anion-assisted ones.

The formation of the honeycomb-like nanoporous Co_3O_4 structures typically involves the following reactions: [65]:

$$CoCl_2 \rightarrow Co^{2+} + 2Cl^- \quad (1)$$

$$(H_2N)^{2-}CO + 2H_2O \rightarrow 2NH_3 + CO_2 \quad (2)$$

$$NH_3 + H_2O \rightarrow NH^{4+} + OH^- \quad (3)$$

$$Co^{2+} + 2OH^- \rightarrow Co(OH)_2 \quad (4)$$

$$3Co(OH)_2 \rightarrow Co_3O_4 + 2H_2O + H_2 \quad (5)$$

During annealing, the $Co(OH)_2$ compound undergoes a thermodynamically unstable state and transforms into the Co_3O_4 phase [66].

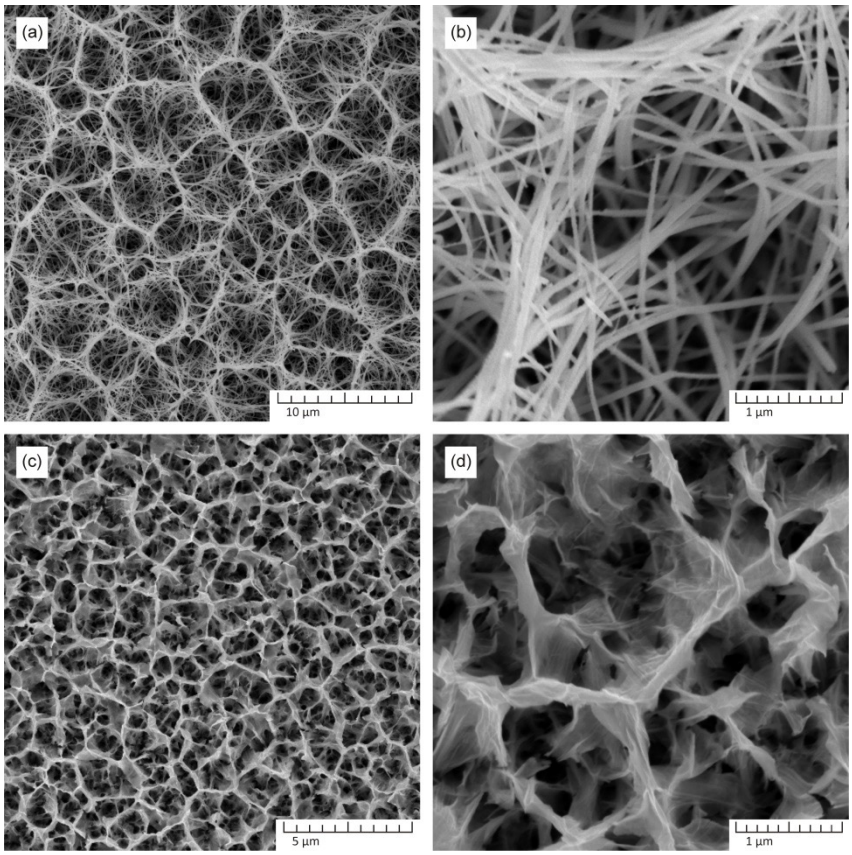

Fig. 1. The study of the anion effect on the morphology of the Co_3O_4 nanostructures. Co_3O_4 nanostructures obtained from the precursor of cobalt chloride and urea (a-b), Co_3O_4 nanostructures obtained from the precursor of cobalt acetate and urea (c–d).

According to [67], a proposed growth mechanism for Co_3O_4 nanowires involves the initial generation of Co nuclei, which gradually undergo a transformation into small nanoparticles. These nanoparticles then serve as nuclei for the growth of larger particles. This growth process is energetically favorable due to a decrease in surface energy as the nanoparticle size increases. To minimize surface energy, the small nanoparticles undergo an aggregation process, leading to the formation of larger nanoparticle aggregates.

The dynamic behavior of these aggregates enables them to move within the solution and come into contact with neighboring nanoparticles. As a result, they merge together, forming short chain structures that act as templates for the formation of elongated rod-like structures. During the later stages of growth, attaching new Co nuclei to existing nanoparticle agglomerates becomes more energetically favorable than creating individual nanoparticles. As a result, the chains formed during this stage further develop into complete nanofibers, exhibiting an increase in linear dimensions based on the growth anisotropy along various crystallographic planes.

Since the nanofibers are quite thin and long, they are not able to maintain a vertical position, so they tilt, meet

with neighboring structures, and continue growing in groups to form a cellular surface structure. The variation in the morphology of nanostructures achieved by using cobalt acetate as the precursor can be elucidated as follows. Acetate ions possess surfactant properties, functioning as capping agents during the growth of nanostructures. These ions contain charged regions that can selectively attach to specific crystallographic planes, impeding growth along those directions and stimulating growth in atypical directions.

In the case of cobalt acetate, the growth of nanofibers in length is hindered as acetate ions block this particular growth direction. Instead, the formation of 2D structures becomes prominent. Moreover, the extensive blocking of numerous crystallographic planes restricts the complete development and enlargement of the initial generation nanostructure. Consequently, recurrent renucleation and attachment occur, resulting in the formation of second-generation nanostructures. These nanostructures are often smaller in size and exhibit lower crystallinity.

As a result, a network of second-generation nanostructures is established, and the overall nanostructured coating possesses reduced crystallinity compared to the original process conducted without acetate ions. This observation is further supported by the X-ray diffraction pattern of the obtained samples (Fig. 2). Specifically, the nanostructures produced with the presence of acetate ions exhibit less prominent peak heights corresponding to crystallographic planes and demonstrate a higher amorphous background.

In addition, EDS microanalysis confirmed the high chemical purity of the obtained samples. The composition of the samples consists of cobalt (47.22 at. %) and oxygen (52.78 at. %) atoms, indicating the absence of any foreign impurities. This analysis further supports the quality and integrity of the Co_3O_4 nanostructures. Figure 2 displays the results of XRD analysis.

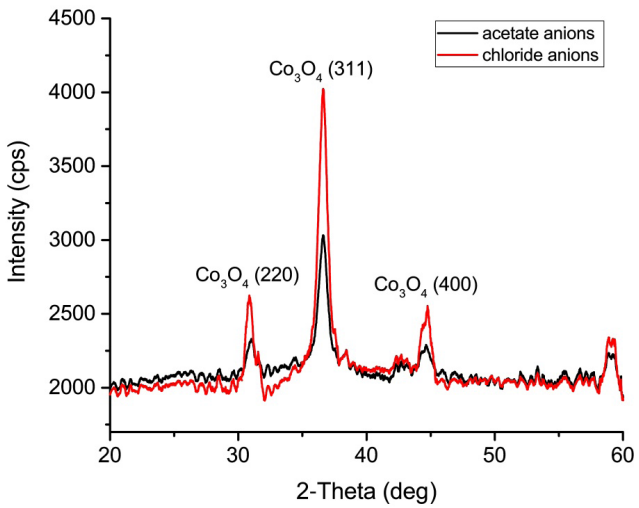

Fig. 2. X-ray diffraction pattern of CO_3O_4 nanostructured samples synthesized via the hydrothermal method. The red and black curves correspond to the chloride anion-assisted structures and the acetate anion-assisted samples, respectively.

The peaks shown in the graph correspond solely to Co_3O_4, indicating a high purity of both samples without any extraneous phase inclusions. While the presence of a background suggests the existence of an amorphous phase, the clear and distinct peaks demonstrate the crystalline nature of the obtained Co_3O_4 nanofibers. The X-ray diffraction pattern exhibits multiple crystallographic planes related to the Co_3O_4 lattice, with the dominant orientation perpendicular to the (3,1,1) planes. As illustrated in Fig. 2, the intensity of the peak for the (3,1,1) plane is higher for the chloride precursor sample than that for the acetate precursor sample, indicating a higher level of crystallinity in the former.

To assess the performance of the nanostructured electrode, cyclic voltammetry (CV) was employed at a scan rate of 100 $mV \cdot s^{-1}$ in a 0.1 M NaOH electrolyte for the detection of H_2O_2. Figure 3a presents the CV results obtained with and without the addition of H_2O_2 to a 0.1 M NaOH buffer solution, focusing on Co_3O_4 nanofibers derived from chloride anions. Notably, the Co_3O_4 modified electrode displayed two distinct pairs of clearly defined redox peaks [68].

In the presence of 0.1 M NaOH, the Co_3O_4 electrode exhibited anodic peaks at approximately -0.8 V (peak I) and -0.15 V (peak II), along with cathodic peaks at around -1.23 V (peak III) and 0.35 V (peak IV). These peaks corresponded to the oxidation and reduction processes of cobalt phases. The reversible transition between

Co_3O_4 and CoOOH was attributed to the redox peak pair I/III, while the further conversion between CoOOH and CoO_2 was ascribed to another redox peak pair II/IV [68]. These two reversible reactions can be described as follows [69]–[71]:

$$Co_3O_4 + OH^- + H_2O \rightarrow 3CoOOH + e^- \quad (6)$$

$$CoOOH + OH^- \rightarrow CoO_2 + H_2O + e^- \quad (7)$$

Upon the addition of 0.2 mM H_2O_2 into the buffer solution, the shape of the CV curve significantly changed with a significant increase in the peak current for the oxidation peak (I) and reduction peak (III).

The peak (III) current value increases linearly with an increase in the concentration of the added H_2O_2. Peak (I) increases less pronouncedly; moreover, with increasing concentration, its position along the x axis shifts, reaching -0.7 V for high concentrations. With the addition of H_2O_2, peak (II) shows no visible changes over the entire range of concentrations. Peak (IV) also changes slightly with the addition of various concentrations of H_2O_2.

The mechanism [68]–[70], [72]–[74] of the electrocatalysis of H_2O_2 is shown in Eq. (8):

$$6CoOOH + H_2O_2 \rightarrow 2Co_3O_4 + O_2 + 4H_2O \quad (8)$$

The CV results for the Co_3O_4 petal-shaped nanostructures obtained from the acetate precursor are shown in Fig. 3b. It can be seen that when peroxide is added, the height of peak (III) is significantly lower than for similar concentrations in the case when fiber-like samples are used (Fig. 3a). This indicates a lower sensitivity and, as a result, the effectiveness of this morphology for H_2O_2 detection. This may be due to the low crystallinity of this morphology and the blocking of active bonds by acetate ions. In addition, the resulting nanopetals are very thin and can stick together under the influence of the weight of the liquid, which significantly reduces the working surface area. Therefore, later in this article, fiber-like nanostructures are considered.

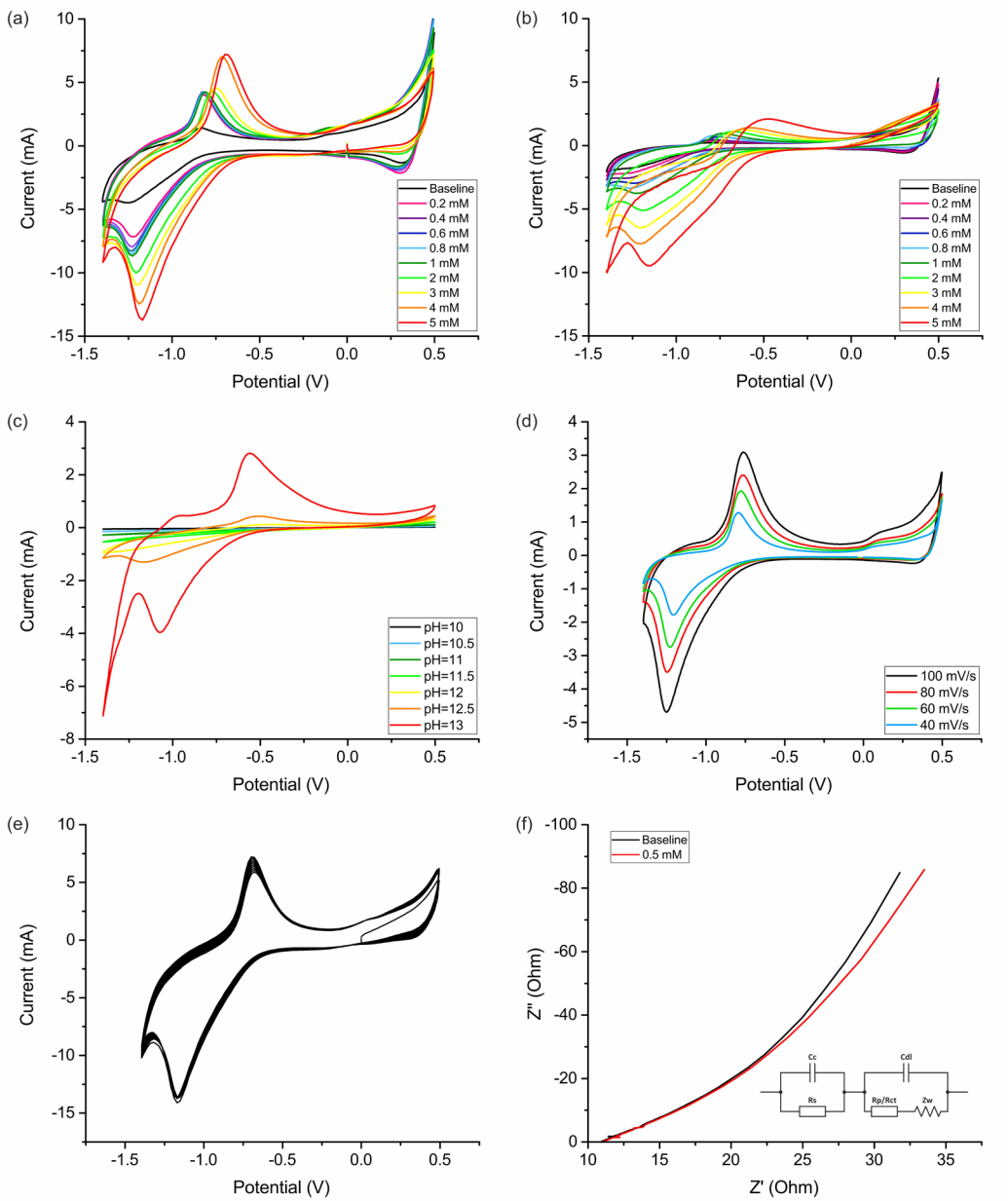

Fig. 3. (a) CV results of a nanostructured Co_3O_4 film derived from chloride anions. Measurements were performed at a scan speed of 100mV/s in a 0.1 M NaOH buffer solution (pH = 13) containing 0-5mM H_2O_2. (b) CV results of a nanostructured Co_3O_4 film derived from acetate anions at the same measurement conditions. (c) The results of CV measurements obtained at different pH values of the buffer solution. Measurements were conducted in NaOH solution containing 5 mM H_2O_2 at a scan rate of 100 mV/s. (d) The results of CV measurements obtained at different scan rates. Measurements were conducted in a 0.1 M NaOH solution containing 5 mM H_2O_2. (e) Working electrode stability study over multiple CV cycles (n = 50). Measurements were conducted in a 0.1 M NaOH solution containing 5 mM H_2O_2. (f) Electrode EIS analysis with a frequency range of 1 Hz to 100 kHz at an applied 0.25V signal voltage. Measurements were conducted in a 0.1 M NaOH solution before and after adding 0.5 mM H_2O_2.

The electrochemical response of Co_3O_4 nanofiber arrays towards 5 mM H_2O_2 was studied using CV at different scan rates ranging from 40 to 100 mV·s-1 (Fig. 3d). It was observed that the electrocatalytic reduction peak current towards H_2O_2 increased with the increase in scan rates. This indicates that the Co_3O_4 nanofiber electrode performs better for H_2O_2 detection at a scan rate of 100 $mV \cdot s^{-1}$.The CV responses of Co_3O_4 nanofiber arrays were examined at numerous concentrations of NaOH with the aim of determining the effect of pH levels of the buffer solution on the sensing effectiveness towards H_2O_2 (Fig. 3d). The absence of characteristic peaks in the pH range of 10 to 11.5 suggests that the electrocatalytic reduction of H_2O_2 is not efficient. The appearance of minimal peaks is observed at pH=12, while the best results with an intense reduction peak and a maximal current value are obtained at pH=13.

Several studies have emphasized the importance of a high pH level in the buffer solution for efficient catalysis of H_2O_2 by transition metal oxide catalysts during the electrochemical process. This leads to an increased cathodic peak current density [69], [75]. Typically, a 0.1 M NaOH or KOH solution suffices to ensure a favorable catalytic response. The presence of OH^- ions, generated from oxyhydroxide products, plays a crucial role in the diffusion process within the nanostructured layer. This enhances the conductivity of the oxyhydroxide, surpassing that of the hydroxide, and promotes a more efficient transfer of charge towards the wire substrate. Consequently, applying a negative potential activates the Co_3O_4 electrode in an alkaline solution, enabling successful detection of H_2O_2 [75].

The stability of the electrode was evaluated over multiple cyclic voltammetry (CV) cycles (n=50), as shown in Figure 3e. It can be observed that the cycles overlap, and the current peak value only undergoes slight changes over time. This indicates that the electrode stabilizes after the second scanning cycle. The minor differences observed during the first scanning cycle can be attributed to wetting processes occurring within the highly porous nanostructured layer.

Figure 3f depicts the electrochemical impedance spectroscopy (EIS) curve obtained before and after adding 0.5 mM H_2O_2, accompanied by the corresponding equivalent circuit. Notably, the absence of characteristic semicircles, formed by the circuit elements' RC components, can be explained by the low charge transfer resistance and the prevalence of Warburg diffusion over other processes within the electrochemical system. The diffusion coefficient, derived from the graph, was found to be $1.237 \cdot 10^{-7}$ $cm^2 \cdot s^{-1}$. The active surface area of the electrode can be determined using Equation (9) from the Randles–Sevcik equation [76]–[78].

$$I_p = (2.69 \cdot 10^5) n^{3/2} A C^* D^{1/2} v^{1/2}, \quad (9)$$

where Ip represents the redox peak current (in μA), n expresses the number of electrons transferred during the redox reaction, A is the effective surface of the working electrode (cm^2), C* is the concentration of NaOH in buffer solution ($mol \cdot cm^{-3}$), D is the solution diffusion coefficient (NaOH = $1.237 \cdot 10^{-7}$ $cm^2 \cdot s^{-1}$) and ν represents the scan rate (100 $mV \cdot s^{-1}$). The calculated electrochemically active surface area was found to be 4.684 cm^2, while the active surface area of the wire without considering the contribution of the nanostructures was 1.256 cm^2. The presence of porous honey-comb-like nanostructured arrays of Co_3O_4, coupled with the large specific surface area, allows for easy electrolyte access and H_2O_2 diffusion towards the

highly available active sites, leading to an improved electrocatalytic process. Typical graphs of the amperometric response for the nanostructured Co_3O_4 electrodes are presented in Figs. 4a and 4b.

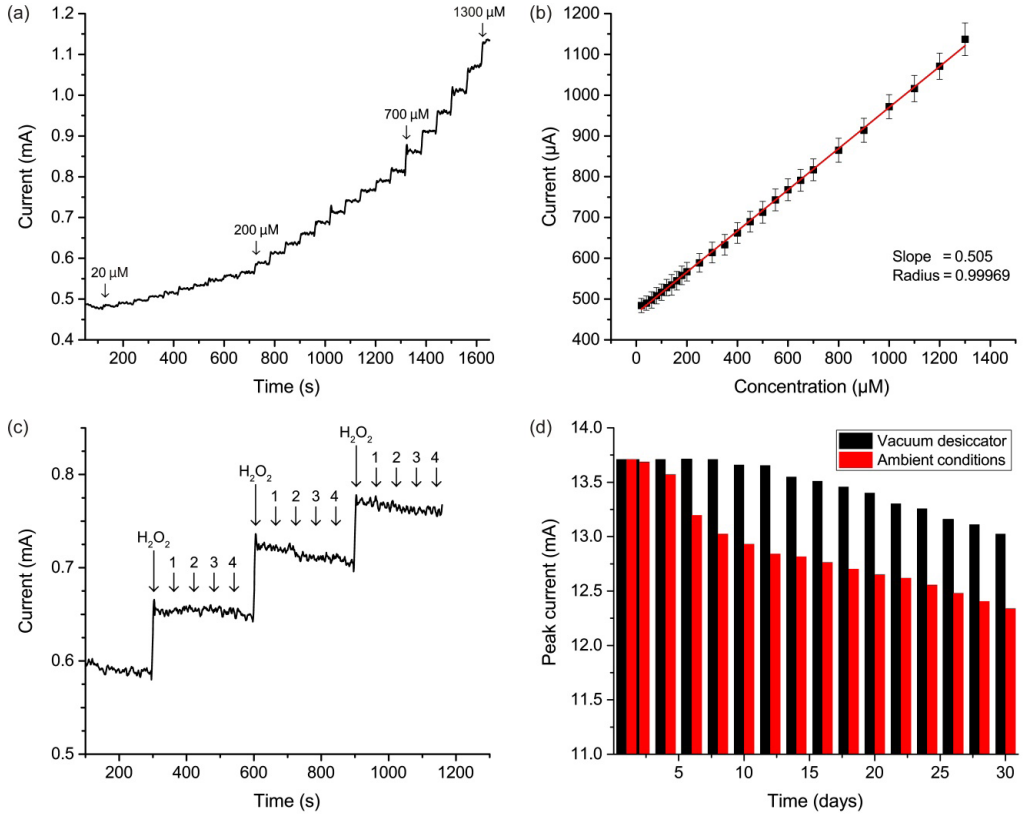

Fig. 4. The figure show (a) the i-t response of the nanostructured Co_3O_4 electrode in 0.1 M NaOH buffer solution with gradual addition of H_2O_2 at concentrations ranging from 20 to 1300 µM, and (b) the corresponding sensor calibration curve. Three steps for the interference study of the nanostructured Co_3O_4 electrode in 0.1 M NaOH is shown in (c) with stepwise addition of H_2O_2 at concentrations ranging from 100 to 300 µM, along with the most common interfering substances, such as (1) ascorbic acid, (2) uric acid, (3) glucose, and (4) NaCl. (d) The stability study is presented for the nanostructured Co_3O_4 samples stored under ambient conditions and in a vacuum desiccator.

Upon addition of H_2O_2, the amperometric response of the nanostructured Co_3O_4 electrode exhibits rapidity, stability, and high sensitivity. The current attains a steady-state value in a matter of seconds and remains relatively constant until the next dose of H_2O_2 is introduced, thereby generating a well-defined current step that is appropriate for determining the current response. The calibration curve depicting the correlation between the catalytic current values and the H_2O_2 concentration in the buffer solution is presented in Fig. 4b. A linear relationship between the current and the concentration of H_2O_2 was observed in a broad range of concentrations spanning from 20 to 1300 µM, with a correlation coefficient (R) of 0.99969. The sensitivity of the Co_3O_4 electrode was determined to be 505.11 $\mu A \cdot mM^{-1}$. By considering a signal-to-

noise ratio of 3, the calculated limit of detection (LOD) was found to be 1.05 μM.

According to publications [79]–[81], for effective milk antibacterial treatment, a minimal H_2O_2 concentration of 0.01 %, which is equivalent to 2.9 mM, is used. This value significantly exceeds the calculated LOD for our sensor. If we consider biomedicine as a potential application of our sensor, the likely range of H_2O_2 in biological fluids (in particular, in blood plasma) is in the range 1–5 μM [82, 83], which is also within the sensitivity of this sensor. This proves the significance of the sensor described in this article for food analysis and further potential applications in healthcare and diagnostics. This sensor can also be successfully used to determine concentrations that are obviously lower than calculated LOD value. In this case, a standard sample recovery test is performed and for this purpose the samples are spiked with different amounts of H_2O_2 above the detection threshold.

To ensure effective application in the analysis of complex analytes, it is crucial to establish high selectivity for the sensor. To achieve this, the selectivity of the Co_3O_4 wire electrode was assessed using four interferents: ascorbic acid, uric acid, glucose, and NaCl. These compounds are commonly present in biological fluids and food products, and are often encountered alongside H_2O_2 in clinical and pharmaceutical applications. They may potentially cause false increasing of amperometric response due to their oxidizing nature and ability to interact with Co_3O_4 nanostructures. Figure 4c shows the amperometric response after introducing 0.1 mM H_2O_2 and 0.1 mM interferent sequentially. The response does not surpass the background noise value, indicating that the nanostructures are not sensitive to these substances and thus confirming the high selectivity of the sensor towards H_2O_2 detection.

To evaluate the long-term stability of the nanostructures, the samples were stored under ambient conditions (20 °C, 40 % relative humidity) for one and four weeks, and CV measurements were taken every two days to assess the stability of the nanostructured electrode by measuring the degree of reduction of the current peak value. The results showed that the signal level remained not less than 95 % of the initial value for samples stored for one week, but decreased to 90 % of the initial value for samples stored for four weeks at ambient condition. Previous studies have suggested that storing CuO and ZnO nanostructures in a vacuum desiccator can significantly reduce sample degradation, so a similar experiment was conducted for Co_3O_4. After a week of storage in the desiccator, the samples did not lose their original electrochemical properties at all, and after a month of storage, they retained 95 % of the initial value of the signal (as shown in Fig. 4d). SEM was used to investigate the influence of storage time on the morphology of the samples, and the results showed no visual changes in the morphology of the nanostructures even after four weeks of storage under ambient conditions. Therefore, it can be concluded that the decrease in sensor sensitivity is mainly due to the adsorption and binding of atmospheric moisture by the developed surface of nanostructures, and this effect can be reduced by storing samples in a vacuum or by preliminary annealing at a temperature of about 100 ºC.

The exceptional stability of these electrodes enables their preparation for future use and the effective preservation of unused electrodes. It is worth emphasizing that the utilization of these electrodes is highly environmentally sustainable and does not contribute to additional waste generation, unlike plastic chips and polymer substrates. The employed electrodes can be easily cleansed of the nanostructured layer through chemical methods or grinding, while the underlying wire can be resurfaced with new nanostructures, enabling its reuse. The results of this study are comparable to those of several published studies where cobalt oxide nanostructures were used for electrode modification for H_2O_2 detection (as summarised in Table 1).

Table 1. Analytical Performance of the Obtained Co_3O_4 Compared to Other Reported Cobalt Oxide Based H_2O_2 Sensors

Electrode	Morphology of nanostructures	Linear range (μM)	Sensitivity ($\mu A \cdot mM^{-1}$)	LOD (μM)	Source
Co_3O_4/GCE	Hollow-sphere	0.4–2200	120.55	0.105	[68]
CoO-CoS/NF	Sheet-like	2–954	590	0.890	[69]
Co_3O_4–rGO/GCE	Wire-like	15–675	456	2.4	[72]
Co-MOF/GCE	Powder	5–9000	83.10	3.76	[73]
Co_3O_4/GCE	Nanocolumns	100–2000	-	0.28	[75]
Co_3O_4 SPCE	Nanourchins	0.1–50	24	0.145	[70]
Co_3O_4@CNBs/GCE	Nanoparticles	0.01–359	-	0.00232	[74]
Co_3O_4 NPs/GE	Nanoparticles	-	-	0.0217	[84]
Co_3O_4/FeWire	Nanowires	20–1300	505.11	1.05	This work

The comparison table reveals that the sensitivity of the electrode discussed in this study is among the highest when compared to other sources. Although the limit of detection (LOD) value is relatively low, there are sources with both higher and lower values than the one reported in this article. However, this is not a significant drawback as the high sensitivity of the material holds the potential for achieving a lower LOD by optimizing the design of a customized electrochemical cell, increasing the working surface area of the electrode, and implementing additional mathematical processing techniques. Furthermore, the spike method described earlier can be employed to determine concentrations below the detection limit.

It is important to emphasize that even with the current performance, the electrode is already suitable for its intended applications since the normal levels of hydrogen peroxide in biological and pharmaceutical samples generally exceed the detection threshold.

Another notable advantage of our electrode compared to others is its accessibility, low cost, and ease of manufacturing. The fabrication methodology eliminates the need for expensive conductive polymers, complex matrices, and costly glassy carbon electrodes (GCE). These factors make our approach highly attractive for potential mass production, promoting wider accessibility to this technology. Furthermore, it is worth emphasizing that most of the sources mentioned employ a surface nanostructuring method that involves applying pre-synthesized nanoparticles in powder form. However, this approach can lead to challenges in achieving repeat-

ability due to the uneven distribution of nanoparticles in the solution and weak adhesion to the electrode surface. In contrast, our novel approach eliminates these drawbacks by utilizing hydrothermal synthesis directly on the electrode surface. This results in a strong, orderly, and uniform epitaxial coating, ensuring enhanced performance and reliability.

The analysis of actual samples using amperometry is documented in Table 2. To account for potential H_2O_2 levels below the detectable range in milk and lens storage solution samples, various quantities of H_2O_2 within a concentration range above the detection threshold were added to each sample. A standard test for sample recovery was then carried out. The findings highlight the electrode's remarkable recovery rate, achieving over 95 % recovery in all instances. Furthermore, the relative standard deviation for the three samples of each spiked concentration remained below 5 %.

Table 2. Results of Determination of Hydrogen Peroxide in Real Milk and Lens Storage Samples

Milk				Contact lens storage solution			
Added (μM)	**Found (μM)**	**Recovery (%)**	**RSD (%) (n = 3)**	**Added (μM)**	**Found (μM)**	**Recovery (%)**	**RSD (%) (n = 3)**
0	-	-	-	0	-	-	-
10	9.51	95.1	5.5	10	9.67	96.7	5.3
25	24.08	96.3	5.1	25	23.89	95.6	5.5
50	47.91	95.8	4.7	50	47.88	95.8	4.4
100	96.25	96.3	4.3	100	97.65	97.7	4.8

If we compare the results obtained in this experiment for the Co_3O_4 nanostructures with the results of previous studies for the CuO nanostructures [85], we can see that cobalt oxide nanostructures show a slightly better sensitivity and long-term stability result; however, its characteristics largely coincide with the CuO coating and likely depend on the geometry and properties of the electrochemical cell. Wire electrodes coated with both oxides are resistant to mechanical and chemical influences and are also characterized by high repeatability in the manufacturing process. However, the position (voltage) of the characteristic peak responsible for the reaction of H_2O_2 with Co_3O_4 nanostructures differs from that for CuO, making it possible to use both oxides in the further development of a multisensor suitable for use in healthcare and food analysis. Multisensor will increase the sensitivity and accuracy of the meaurement compared to using a single working electrode due to cross sensitivity of various metal oxides, as well as expand the areas of application and the list of analyzed analytes supplementing the list of obtainable electrodes with other metal oxides (for example, NiO, TiO_2, ZnO, Fe_3O_4 and others). Applying cross sensitivity also make it possible to detect several analytes simultaneously and study their interactions in real samples with a complex composition.

5. CONCLUSIONS

This article presents the synthesis of a nanostructured coating composed of Co_3O_4, using the hydrothermal method directly on the surface of Fe wire electrode and its practical application as a working electrode for the electrochemical detection of H_2O_2 in real samples with a complex chemical composition. The resulting coating exhibits high homogeneity and excellent adhesion to the iron wire, ensuring its mechanical and chemical resistance during sample processing and electrochemical measurements. The nanostructured Co_3O_4 coating displays a honeycomb-shaped surface, which exhibits significant peroxidase-like electrocatalytic activity, enabling the detection of H_2O_2 with high sensitivity over a wide range of concentrations. The study demonstrates that the morphology of the nanostructures is strongly dependent on the precursor's chemical composition. Thus, the chloride anions provide the formation of fiber-like nanostructures, while the acetate anions under similar growth conditions provide the formation of thin petal-like nanostructures of Co_3O_4. It has been found that fiber-like nanostructures of Co_3O_4 have better sensory characteristics compared to petal-like samples and are more efficient for electrochemical detecting of H_2O_2. It has also been determined that the efficiency of this sensor increases with an increase in the scanning speed and an increase in the pH of the buffer solution.

The resulting electrode exhibits a linear current response over a wide concentration range of 20 to 1300 μM, with a sensitivity of 505.11 $\mu A \cdot mM^{-1}$ and a calculated LOD of 1.05 μM. The electrochemically active surface area is determined to be 4.684 cm^2. Interference tests reveal that the sensor is highly selective, with no electrochemical response to the most common interfering substances. The long-term stability study shows that the signal level remains at 95 % of the initial current value after one week and at 90 % after four weeks of storage under ambient conditions. However, the electrode lifespan can be significantly improved by storing it in a vacuum desiccator until they are needed. In this case, the signal level remains at 100 % of the initial value after one week and at 95 % after four weeks.

The milk and lens storage liquid analysis has demonstrated a high recovery rate of over 95 %, indicating that this sensor is suitable for quantitative and qualitative deermination of H_2O_2 in real samples with complex compositions.

Further research will be aimed at studying this sensor for healthcare applications to analyse changes in the concentration of H_2O_2 in biological fluids (in particular, in blood plasma). Since our research group has already had an experience in creating similar sensors based on other metal oxides (in particular, CuO, Fe_3O_4, NiO), the next promising application will be the integration of this sensor into a multisensor system. The use of a multisensor will increase the sensitivity compared to the use of each oxide separately due to cross-sensitivity and will also expand the range of possible analytes and will allow samples of a more complex composition to be studied. It will also be possible to target the detection of several analytes simultaneously, which is very important in the field of healthcare for monitoring certain diseases.

ACKNOWLEDGEMENTS

The research has been supported by ESF Project No. 8.2.2.0/20/I/003 "Strengthening of Professional Competence of Daugavpils University Academic Personnel of Strategic Specialization Branches 3rd Call".

REFERENCES

1. Dhara, K., & Mahapatra, D.R. (2019). Recent Advances in Electrochemical Nonenzymatic Hydrogen Peroxide Sensors Based on Nanomaterials: A Review. J. *Mater. Sci., 54*, 12319–12357. https://doi.org/10.1007/s10853-019-03750-y
2. Mohanan, P.V., Sangeetha, V., Sabareeswaran, A., Muraleedharan, V., Jithin, K., Vandana, U., & Varsha, S.B. (2021). Safety of 0.5% Hydrogen Peroxide Mist Used in the Disinfectiongateway for COVID-19. *Environ. Sci. Pollut. Res. Int., 28* (47), 66602–66612. https://doi.org/10.1007/s11356-021-15164-y
3. SCCP (Scientific Committee on Consumer Products). (2007). *Opinion on Hydrogen Peroxide, in its Free Form or when Released, in Oral Hygiene Products and Tooth Whitening Products.* Available at https://ec.europa.eu/health/ph_risk/committees/04_sccp/docs/sccp_o_122.pdf
4. National Center for Biotechnology Information. (2022). *PubChem Compound Summary for CID 784, Hydrogen Peroxide*. Available at https://pubchem.ncbi.nlm.nih.gov/compound/Hydrogen-Peroxide
5. Mahaseth, T., & Kuzminov, A. (2016). Potentiation of Hydrogen Peroxide Toxicity: From Catalase Inhibition to Stable DNA-Iron Complexes. *Mutat. Res.: Rev. Mutat. Res. 773*, 274–281. https://doi.org/10.1016/j.mrrev.2016.08.006
6. Schnabel, T., Mehling, S., Londong, J., & Springer, C. (2020). Hydrogen Peroxide-Assisted Photocatalytic Water Treatment for the Removal of Anthropogenic Trace Substances from the Effluent of Wastewater Treatment Plants. *Water Sci. Technol. 82* (10), 2019–2028. https://doi.org/ 10.2166/wst.2020.481
7. Ksibi, M. (2006). Chemical Oxidation with Hydrogen Peroxide for Domestic Wastewater Treatment. *Chem. Eng. J.*, *119* (2–3), 161–165. https://doi.org/10.1016/j.cej.2006.03.022
8. Xu, J., Zheng, X., Feng, Z., Lu, Z., Zhang, Z., Huang, W., ... & Cui, Y. (2021). Organic Wastewater Treatment by a Single-Atom Catalyst and Electrolytically Produced H_2O_2. *Nat. Sustain., 4*, 233–241. https://doi.org/10.1038/s41893-020-00635-w
9. Arefin, S., Sarker, M.A.H., Islam, M.A., Harun-ur-Rashid, M., & Islam, M.N. (2017). Use of Hydrogen Peroxide (H_2O_2) in Raw Cow's Milk Preservation. *J. Adv. Vet. Anim. Res. 4* (4), 371–377. https://doi.org/10.5455/javar.2017.d236
10. Silva, E., Oliveira, J., Silva, Y., Urbano, S., Sales, D., Moraes, E., … & Anaya, K. (2020). Lactoperoxidase System in the Dairy Industry: Challenges and Opportunities. *Czech J. Food Sci. 38*, 337–346. https://doi.org/ 10.17221/103/2020-CJFS
11. Gaikwad, R., Thangaraj, P.R., & Sen, A.K. (2021). Direct and Rapid Measurement of Hydrogen Peroxide in Human Blood Using a Microfluidic Device. *Sci. Rep. 11* (1), 112960 https://doi.org/10.1038/s41598-021-82623-4
12. Totsuka, K., Ueta, T., Uchida, T., Roggia, M.F., Nakagawa, S., Vavvas, D.G., ... & Aihara, M. (2019). Oxidative Stress Induces Ferroptotic Cell Death in Retinal Pigment Epithelial Cells. *Exp. Eye Res. 181*, 316–324. https://doi.org/10.1016/j.exer.2018.08.019
13. Whittemore, E.R., Loo, D.T., Watt, J.A., & Cotman, C.W. (1995). A Detailed Analysis of Hydrogen Peroxide-Inducded Cell Death in Primary Neuronal Culture. *Neurosci. 67* (4), 921–932. https://doi.org/10.1016/0306-4522(95)00108-u

14. Guesmi, F., Bellamine, H., & Landoulsi, A. (2018). H2O2-Induced Oxidative Stress, AChE Inhibition and Mediated Brain Injury Attenuated by *Thymus algeriensis*. *Appl. Physiol. Nutr. Metab.*, *43* (12), 1275–1281. https://doi.org/10.1139/apnm-2018-0107

15. Dev, S., Kumari, S., Singh, N., Bal, S.K., Seth, P., & Mukhopadhyay, C. K. (2015). Role of Extracellular Hydrogen Peroxide in Regulation of Iron Home- Ostasis Genes in Neuronal Cells: Implication in Iron Accumulation. *Free Radic. Biol. Med., 86,* 78–89. https://doi.org/10.1016/j.freeradbiomed.2015.05.025

16. Tabner, B.J., El-Agnaf, O.M.A., Turnbull, S., German, M.J., Paleologou, K.E., Hayashi, Y., … & Allsop, D. (2005). Hydrogen Peroxide Is Generated during the Very Early Stages of Aggregation of the Amyloid Peptides Implicated in Alzheimer Disease and Familial British Dementia. *J. Biol. Chem., 280* (43), 35789–35792. https://doi.org/10.1074/jbc.C500238200

17. Lee, S., Lee, Y.J., Kim, J.H., & Lee, G. (2020). Electrochemical Detection of H_2O_2 Released from Prostate Cancer Cells Using Pt Nanoparticle-Decorated rGO–CNT Nanocomposite-Modified Screen-Printed Carbon Electrodes. *Chemosensors 8* (3), 63. https://doi.org/10.3390/chemosensors8030063

18. Kolbasina, N.A., Gureev, A.P., Serzhantova, O.V., Mikhailov, A.A., Moshurov, I.P., Starkov, A.A., & Popov, V.N. (2020). Lung Cancer Increases H2O2 Concentration in the Exhaled Breath Condensate, Extent of mtDNA Damage, and mtDNA Copy Number in Buccal Mucosa. *Heliyon, 6* (6), e04303. https://doi.org/10.1016/j.heliyon.2020.e04303

19. Abdalla, A., Jones, W., Flint, M.S., & Patel, B.A. (2021). Bicomponent Composite Electrochemical Sensors for Sustained Monitoring of Hydrogen Peroxide in Breast Cancer Cells. *Electrochim. Acta, 398*, 139314. https://doi.org/10.1016/j.electacta.2021.139314

20. Tavakkoli, H., Akhond, M., Ghorbankhani, G.A., & Absalan, G. (2020). Electrochemical Sensing of Hydrogen Peroxide Using a Glassy Carbon Electrode Modified with Multiwalled Carbon Nanotubes and Zein Nanoparticle Composites: Application to HepG2 Cancer Cell Detection. *Microchim. Actam, 187*, 105. https://doi.org/10.1007/s00604-019-4064-7

21. Wu, Y., Guo, T., Qiu, Y., Lin, Y., Yao, Y., Lian, W., ... & Yang, H. (2019). An Inorganic Prodrug, Tellurium Nanowires with Enhanced ROS Generation and GSH Depletion for Selective Cancer Therapy. *Chem. Sci. 10* (29), 7068–7075. https://doi.org/10.1039/c9sc01070j

22. Ahmad, T., Iqbal, A., Halim, S.A., Uddin, J., Khan, A., El Deeb, S., & Al-Harrasi, A. (2022). Recent Advances in Electrochemical Sensing of Hydrogen Peroxide (H_2O_2) Released from Cancer Cells. *Nanomaterials, 12* (9), 1475. https://doi.org/10.3390/nano12091475

23. Maier, D., Laubender, E., Basavanna, A., Schumann, S., Güder, F., Urban, G.A., & Dincer, C. (2019). Toward Continuous Monitoring of Breath Biochemistry: A Paper-Based Wearable Sensor for Real-Time Hydrogen Peroxide Measurement in Simulated Breath. *ACS Sens., 4* (11), 2945–2951. https://doi.org/10.1021/acssensors.9b01403

24. Xie, J., Cheng, D., Zhou, Z., Pang, X., Liu, M., Yin, P., ... & Yao, S. (2020). Hydrogen Peroxide Sensing in Body Fluids and Tumor Cells via In situ Produced Redox couples on Two-dimensional Holey $CuCo_2O_4$ Nanosheets. *Microchim. Acta, 187* (8), 469. https://doi.org/10.1007/s00604-020-04389-2

25. Kakeshpour, T., Metaferia, B., Zare, R.N., & Bax, A. (2022). Quantitative Detection of Hydrogen Peroxide in Rain, Air, Exhaled Breath, and Biological Fluids by NMR Spectroscopy. *Proc. Natl. Acad. Sci. U.S.A. 119* (8), e2121542119. https://doi.org/10.1073/pnas.2121542119

26. Liu, H., Weng, L., & Yang, C. (2017). A Review on Nanomaterial-Based Electrochemical Sensors for H_2O_2, H_2S and NO inside Cells or Released by Cells. *Microchim. Acta, 1847,* 1267–1283. https://doi.org/10.1007/s00604-017-2179-2

27. Perini, J.A.d.L., Silva, B.C.e., Tonetti, A.L., & Nogueira, R.F.P. (2017). Photo-Fenton Degradation of the Pharmaceuticals Ciprofloxacin and Fluoxetine after Anaerobic Pre-treatment of Hospital Effluent. *Environ. Sci. Pollut. Res., 24,* 6233–6240. https://doi.org/10.1007/s11356-016-7416-4

28. Al-Awadie, N.S.T., & Khudhair, A.F. (2015). Determination of Hydrogen Peroxide in Some Local Pharmaceutical Disinfectants by Continuous Flow Injection Analysis via Turbidimetric ($T_{180}°$) and Scattered Light Effect at Two Opposite Positions ($2N_{90}°$) Using Ayah $4S_W$-3D-$T_{180}°$ -$2N_{90}°$ -Solar - CFI Analyser. *Iraqi J. Sci.*, *56* (1C), 577–592.
29. Payal, A., Krishnamoorthy, S., Elumalai, A., Moses, J.A., & Anandharamakrishnan, C. (2021). A Review on Recent Developments and Applications of Nanozymes in Food Safety and Quality Analysis. *Food Anal. Methods*, *14,* 1537–1558. https://doi.org/10.1007/s12161-021-01983-9
30. Chen, Q., Lin, T., Huang, J., Chen, Y., Guo, L., & Fu, F. (2018). Colorimetric Detection of Residual Hydrogen Peroxide in Soaked Food Based on Au@Ag Nanorods. *Anal. Methods, 10,* 504–507. https://doi.org/10.1039/C7AY02819A
31. Navale, D., & Gupta, S. (2019). Detection of Adultered Formalin and Hydrogen Peroxide in Milk. *JLTEMAS*, *8* (8), 19–21.
32. Vasconcelos, H., Matias, A., Jorge, P., Saraiva, C., Mendes, J., Araújo, J., … & Coelho, L.C.C. (2021). Optical Biosensor for the Detection of Hydrogen Peroxide in Milk. *Chem. Proc., 5* (1), 55. https://doi.org/10.3390/CSAC2021-10466
33. Huang, Y., Wang, L., Chen, B., Zhang, Q., & Zhu, R. (2020). Detecting Hydrogen Peroxide Reliably in Water via Ion Chromatography: A Method Evaluation Update and Comparison in the Presence of Interfering Components. *Environ. Sci.: Water Res. Technol., 6,* 2396–2404. https://doi.org/10.1039/d0ew00234h
34. Su, J., Zhang, S., Wang, C., Li, M., Wang, J., Su, F., & Wang, Z. (2021). A Fast and Efficient Method for Detecting H_2O_2 by a Dual-Locked Model Chemosensor. *ACS Omega, 6* (23), 14819–14823. https://doi.org/10.1021/acsomega.1c00384
35. Fong, D., & Swager, T.M. (2021). Trace Detection of Hydrogen Peroxide via Dynamic Double Emulsions. *J. Am. Chem. Soc., 143* (11), 4397–4404. https://doi.org/10.1021/jacs.1c00683
36. Ito, E., Watabe, S., Morikawa, M., Kodama, H., Okada, R., & Miura, T. (2013). Detection of H_2O_2 by fluorescence correlation spectroscopy. In E. Cadenas, L. Packer (eds.), *Hydrogen Peroxide and Cell Signaling, Part A* (pp 135–143). Academic Press: Cambridge, Massachusetts. https://doi.org/10.1016/B978-0-12-405883-5.00008-9
37. Rezende, F., Brandes, R.P., & Schröder, K. (2018). Detection of H_2O_2 with Fluorescent Dyes. *Antioxid. Redox Signal.*, *29* (6), 585–602. https://doi.org/10.1089/ars.2017.7401
38. Teodoro, K.B.R., Migliorini, F.L., Christinelli, W.A., & Correa, D.S. (2019). Detection of Hydrogen Peroxide (H_2O_2) Using a Colorimetric Sensor Based on Cellulose Nanowhiskers and Silver Nanoparticles. *Carbohydrate Polymers, 212*, 235–241. https://doi.org/10.1016/j.carbpol.2019.02.053
39. Zhu, P., Xu, Z., Cai, L., & Chen, J. (2021). Porphyrin Iron-Grafted Mesoporous Silica Composites for Drug Delivery, Dye Degradation and Colorimetric Detection of Hydrogen Peroxide. *Nanoscale Res. Lett., 16* (1), 41. https://doi.org/10.1186/s11671-021-03501-6
40. Moßhammer, M., Kühl, M., & Koren, K. (2017). Possibilities and Challenges for Quantitative Optical Sensing of Hydrogen Peroxide. *Chemosensors*, *5*, 28. https://doi.org/10.3390/chemosensors5040028
41. Gričar, E., Kalcher, K., Genorio, B., & Kolar, M. (2021). Highly Sensitive Amperometric Detection of Hydrogen Peroxide in Saliva Based on N-Doped Graphene Nanoribbons and MnO_2 Modified Carbon Paste Electrodes. *Sensors, 21*, 8301. https://doi.org/10.3390/s21248301
42. Gorduk, O., Gorduk, S., & Sahin, Y. (2020). Fabrication of Tetra-Substituted Copper(II) Phthalocyanine-Graphene Modified Pencil Graphite Electrode for Amperometric Detection of Hydrogen Peroxide. *ECS J. Solid State Sci. Technol., 9,* 06103. https://doi.org/10.1149/2162-8777/ab9c7a
43. Wang, Q., Zhang, X., Chai, X., Wang, T., Cao, T., Li, Y., & Qi, W. (2021). An Electrochemical Sensor for H_2O_2 Based on Au Nanoparticles Embedded in UiO-66 Metal−Organic Framework Films. *ACS Appl. Nano Mater.*, *4* (6), 6103–6110. https://doi.org/10.1021/acsanm.1c00915

44. Bao-Kai, M., Mian, L., Ling-Zhi, C., Xin-Chu, W., Cai, S., & Qing, H. (2020). Enzyme-MXene Nanosheets: Fabrication and Application in Electrochemical Detection of H_2O_2. *J. Inorg. Mater., 35* (1), 131–138. https://doi.org/10.15541/jim20190139

45. Yu, Y., Pan, M., Peng, J., Hu, D., Hao, Y., & Qian, Z. (2020). A Review on Recent Advances in Hydrogen Peroxide Electrochemical Sensors for Applications in Cell Detection. *Chin. Chem. Lett., 33,* (9), 4133–4145. https://doi.org/10.1016/j.cclet.2022.02.045

46. Portorreal-Bottier, A., Gutiérrez-Tarriño, S., Calventea, J.J., Andreu, R., Roldán, E., Oña-Burgos, P., & Olloqui-Sariego, J.L. (2022). Enzyme-like Activity of Cobalt-MOF Nanosheets for Hydrogen Peroxide Electrochemical Sensing. *Sens. Actuat. B Chem., 368,* 132129. https://doi.org/10.1016/j.snb.2022.132129

47. Bollella, P., & Gorton, L. (2018). Enzyme Based Amperometric Biosensors. *Curr. Opin. Electrochem., 10,* 157–173. https://doi.org/10.1016/j.coelec.2018.06.003

48. Olloqui-Sariego, J.L., Calvente, J.J., & Andreu, R. (2021). Immobilizing Redox Enzymes at Mesoporous and Nanostructured Electrodes. *Curr. Opin. Electrochem., 26,* 100658. https://doi.org/10.1016/j.coelec.2020.100658

49. Nestor, U., Frodouard, H., & Theoneste, M. (2021). A Brief Review of How to Construct an Enzyme-Based H_2O_2 Sensor Involved in Nanomaterials. *Adv. Nanopart., 10*, 1–25. https://doi.org/10.4236/anp.2021.101001

50. Sardaremelli, S., Hasanzadeh, M., & Seidi, F. (2021). Enzymatic Recognition of Hydrogen Peroxide (H_2O_2) in Human Plasma Samples Using HRP Immobilized on the Surface of Poly(arginine-toluidine blue)- Fe_3O_4 Nanoparticles Modified Polydopamine; A Novel Biosensor. *J. Mol. Recognit., 34* (11), e2928. https://doi.org/10.1002/jmr.2928

51. Wu, Z., Sun, L.P., Zhou, Z., Li, Q., Huo, L.H., & Zhao, H. (2018). Efficient Nonenzymatic H_2O_2 Biosensor Based on ZIF-67 MOF Derived Co Nanoparticles Embedded N-doped Mesoporous Carbon Composites. *Sens. Actuat. B Chem., 276*, 142–149. https://doi.org/10.1016/j.snb.2018.08.100

52. Heydaryan, K., Kashi, M.A., Sarifi, N., & Ranjbar-Azada, M. (2020). Efficiency Improvement in Non-enzymatic H_2O_2 Detection Induced by the Simultaneous Synthesis of Au and Ag Nanoparticles in an RGO/Au/Fe_3O_4/Ag Nanocomposite. *New J. Chem., 44*, 9037–9045. https://doi.org/10.1039/d0nj00526f

53. Rashed, M.A., Faisal, M., Harraz, F.A., Jalalah, M., Alsaiari, M., & Alsareii, S.A. (2021). A Highly Efficient Nonenzymatic Hydrogen Peroxide Electrochemical Sensor Using Mesoporous Carbon Doped ZnO Nanocomposite. *J. Electrochem. Soc., 168* (2), 027512. https://doi.org/10.1149/1945-7111/abe44b

54. Nishan, U., Niaz, A., Muhammad, N., Asad, M., Shah, A.-u.-H.A., Khan, N., … & Rahim, A. (2021). Non-enzymatic Colorimetric Biosensor for Hydrogen Peroxide Using Lignin-Based Silver Nanoparticles Tuned with Ionic Liquid as a Peroxidase Mimic. *Arabian J. Chem., 14* (6), 103164. https://doi.org/10.1016/j.arabjc.2021.103164

55. Bukkitgar, S.D., Kumar, P.S., Singh, S., Singh, V., Reddy, K.R., Sadhu, V., … & Naveen, S. (2020). Functional Nanostructured Metal Oxides and its Hybrid Electrodes – Recent Advancements in Electrochemical Biosensing Applications. *Microchem. J.*, *159*, 105522. https://doi.org/10.1016/j.microc.2020.105522

56. Chang, Y.S., Li, J.H., Chen, Y.C., Ho, W.H., Song, Y.D., & Kung, C.W. (2020). Electrodeposition of Pore-Confined Cobalt in Metaleorganic Framework Thin Films toward Electrochemical H_2O_2 Detection. *Electrochim. Acta, 347*, 136276. https://doi.org/10.1016/j.electacta.2020.136276

57. Agnihotri, A. S., Varghese, A., & Nidhin, M. (2021). Transition Metal Oxides in Electrochemical and Bio Sensing: A State-of-Art Review. *Appl. Surf. Sci. Adv., 4,* 100072. https://doi.org/10.1016/j.apsadv.2021.100072

58. Tammineni, V.S., Espenti, C.S., Mutyala, S., & Arunachalam, S.V. (2021). Metal oxide-modified electrochemical sensors for toxic chemicals. In A. Pandikumar & P. Rameshkumar (eds.), *Metal Oxides in Nanocomposite-Based Electrochemical Sensors for Toxic Chemicals* (pp. 19–49). Elsevier Science: Amsterdam. https://doi.org/10.1016/B978-0-12-820727-7.00009-4

59. Trujillo, R.M., Barraza, D.E., Zamora, M.L., Cattani-Scholz, A., & Madrid, R.E. (2021). Nanostructures in Hydrogen Peroxide Sensing. *Sensors, 21* (6), 2204. https://doi.org/10.3390/s21062204

60. Alsaiari, M., Younus, A.R., Rahim, A., Alsaiari, R., & Muhammad, N. (2021). An Electrochemical Sensing Platform of Cobalt Oxide@SiO_2/C Mesoporous Composite for the Selective Determination of Hydrazine in Environmental Samples. *Microchem. J., 165,* 106171. https://doi.org/10.1016/j.microc.2021.106171

61. Kogularasu, S., Govindasamy, M., Chen, S.M., Akilarasan, M., & Mania, V. (2017). 3D Graphene Oxide-Cobalt Oxide Polyhedrons for Highly Sensitive Non-Enzymatic Electrochemical Determination of Hydrogen Peroxide. *Sens. Actuat. B Chem., 253,* 773–783. https://doi.org/10.1016/j.snb.2017.06.172

62. Kumarage, G.W.C., & Comini, E. (2021). Low-Dimensional Nanostructures Based on Cobalt Oxide (Co_3O_4) in Chemical-Gas Sensing. *Chemosensors, 9* (8), 197. https://doi.org/10.3390/chemosensors9080197

63. Rabani, I., Yoo, J., Kim, H.S., Lam, D.V., Hussain, S., Karuppasamy, K., & Seo, Y.S. (2021). Highly Dispersive Co_3O_4 Nanoparticles Incorporated into a Cellulose Nanofiber for a High-performance Flexible Supercapacitor. *Nanoscale 13,* 355–370. https://doi.org/doi.org/10.1039/d0nr06982e

64. Fan, Y., Chen, H., Li, Y., Zheng, D.C., & Xue, F.C. (2021). PANI-Co_3O_4 with Excellent Specific Capacitance as an Electrode for Supercapacitors. *Ceram. Int., 47* (6), 8433–8440. https://doi.org/10.1016/j.ceramint.2020.11.208

65. Ibupoto, Z.H., Elhag, S., AlSalhi, M.S., Nur, O., & Willander, M. (2014). Effect of Urea on the Morphology of Co_3O_4 Nanostructures and Their Application for Potentiometric Glucose Biosensor. *Electroanalysis, 26* (8), 1773–1781. https://doi.org/10.1002/elan.201400116

66. Hussain, M., Ibupoto, Z.H., Abbasi, M.A., Nur, O., & Willander, M. (2014). Effect of Anions on the Morphology of Co_3O_4 Nanostructures Grown by Hydrothermal Method and their pH Sensing Application. *J. Electroanal. Chem., 717–718*, 78–82. https://doi.org/10.1016/j.jelechem.2014.01.011

67. Kannan, P., Maiyalagan, T., Marsili, E., Ghosh, S., Guo, L., Huang, Y., … & Jönsson-Niedziolka, M. (2017). Highly Active 3-Dimensional Cobalt Oxide Nanostructures on the Flexible Carbon Substrates for Enzymeless Glucose Sensing. *Analyst, 142*, 4299–4307. https://doi.org/10.1039/c7an01084b

68. Wang, M., Jiang, X., Liu, J., Guo, H., & Liu, C. (2015). Highly Sensitive H_2O_2 Sensor Based on Co_3O_4 Hollow Sphere Prepared via a Template-Free Method. *Electrochim. Acta, 182,* 613–620. https://doi.org/10.1016/j.electacta.2015.08.116

69. Mai, L.N.T., Bui, Q.B., Bachc, L.G., & Nhac-Vu, H.-T. (2020). A Novel Nanohybrid of Cobalt Oxide-Sulfide Nanosheets Deposited Three-Dimensional Foam as Efficient Sensor for Hydrogen Peroxide Detection. *J. Electroanal.l Chem., 857*, 113757. https://doi.org/10.1016/j.jelechem.2019.113757

70. Barkaoui, S., Haddaoui, M., Dhaouadi, H., Raouafi, N., & Touati, F. (2015). Hydrothermal Synthesis of Urchin-like Co_3O_4 Nanostructures and their Electrochemical Sensing Performance of H_2O_2. *J. Solid State Chem., 228*, 226–231. https://doi.org/10.1016/j.jssc.2015.04.043

71. Shahid, M.M., Rameshkumar, P., & Huang, N.M. (2015). Morphology Dependent Electrocatalytic Properties of Hydrothermally Synthesized Cobalt Oxide Nanostructures. *Ceram. Int. 41* (10), 13210–13217. https://doi.org/ 10.1016/j.ceramint.2015.07.098

72. Kong, L., Ren, Z., Zheng, N., Du, S., Wu, J., Tang, J., & Fu, H. (2014). Interconnected 1D Co_3O_4 Nanowires on Reduced Grapheme Oxide for Enzymeless H_2O_2 Detection. *Nano Res., 8* (2), 469–480. https://doi.org/10.1007/s12274-014-0617-6

73. Yang, L., Xu, C., Ye, W., & Liu, W. (2015). An Electrochemical Sensor for H_2O_2 Based on a New Co-Metal-Organic Framework Modified Electrode. *Sens. Actuat. B Chem., 215*, 489–496. https://doi.org/10.1016/j.snb.2015.03.104

74. Xiong, L., Zhang, Y., Wu, S., Chen, F., Lei, L., Yu, L., & Li, C. Co_3O_4 Nanoparticles Uniformly Dispersed in Rational Porous Carbon Nano-Boxes for Significantly Enhanced Electrocatalytic Detection of H_2O_2 Released from Living Cells. *Int. J. Mol. Sci., 23* (7), 3799. https://doi.org/10.3390/ijms23073799

75. Kannan, P., Maiyalagan, T., Pandikumar, A., Guo, L., Veerakumar, P., & Rameshkumar, P. (2019). Highly Sensitive Enzyme-free Amperometric Sensing of Hydrogen Peroxide in Real Samples Based on Co_3O_4 Nanocolumn Structures. *Anal. Methods, 11*, 2292–2302. https://doi.org/10.1039/c9ay00230h

76. Atacan, K.J. (2019). $CuFe_2O_4$/Reduced Graphene Oxide Nanocomposite Decorated with Gold Nanoparticles as a New Electrochemical Sensor Material for L-cysteine Detection. *Alloys Compd., 791*, 391–401. https://doi.org/10.1016/j.jallcom.2019.03.303

77. Demir, N., Atacan, K., Ozmen, M., & Bas, S.Z. (2020). Design of a New Electrochemical Sensing System Based on MoS_2-TiO_2/Reduced Graphene Oxide Nanocomposite for Paracetamol Detection. *New J. Chem., 44* (27), 11759–11767. https://doi.org/10.1039/d0nj02298e

78. Dhulkefl, A.J., Atacan, K., Bas, S.Z., & Ozmen, M. (2020). Ag-TiO_2-Reduced Graphene Oxide Hybrid Film for Electrochemical Detection of 8-hydroxy-2'-Deoxyguanosine as an Oxidative DNA Damage Biomarker. *Anal. Methods, 12* (4), 499–506. https://doi.org/10.1039/c9ay02175b

79. Arefin, S., Sarker, M.A.H., Islam, M.A., Harun-ur-Rashid, M., & Islam, M.N. (2017). Use of Hydrogen Peroxide (H_2O_2) in Raw Cow's Milk Preservation. *J. Adv. Vet. Anim. Res., 4* (4), 371–377. https://doi.org/10.5455/javar.2017.d236

80. Saha, B.K., Ali, M.Y., Chakraborty, M., Islam, Z., & Hira, A.K. (2003). Study of the Preservation of Raw Milk with Hydrogen Peroxide (H_2O_2) for Rural Dairy Farmers. *Pakistan J. Nutrition, 2* (1), 36–42. https://doi.org/ 10.3923/pjn.2003.36.42

81. Dashe, D., Hansen, E.B., Kurtu, M.Y., Berhe, T., Eshetu, M., Hailu, Y., … & Shegaw, A. (2020). Preservation of Raw Camel Milk by Lactoperoxidase System Using Hydrogen Peroxide Producing Lactic Acid Bacteria. *Open J. Anim. Sci., 10,* 387–401. https://doi.org/10.4236/ojas.2020.103024

82. Forman, H.J., Bernardo, A., & Davies, K.J.A. (2016). Corrigendum to "What is the Concentration of Hydrogen Peroxide in Blood and Plasma?". *Arch. Biochem. Biophys., 603*, 48–53. https://doi.org/10.1016/j.abb.2016.05.005

83. Atta, N.F., Gawad, S.A.A., Galal, A., Razik, A.A., & El-Gohary, A.R.M. (2021). Efficient Electrochemical Sensor for Determination of H_2O_2 in Human Serum Based on Nano Iron/Nickel Alloy/Carbon Nanotubes/Ionic Liquid Crystal Composite. *J. Electroanal. Chem., 881*, 114953. https://doi.org/10.1016/j.jelechem.2020.114953

84. Das, R.K., & Golder, A.K. (2017). Co_3O_4 Spinel Nanoparticles Decorated Graphite Electrode: Bio-mediated Synthesis and Electrochemical H_2O_2 Sensing. *Electrochim. Acta, 251,* 415–426. https://doi.org/10.1016/j.electacta.2017.08.122

85. Mihailova, I., Gerbreders, V., Krasovska, M., Sledevskis, E., Mizers, V., Bulanovs, A., & Ogurcovs, A. (2022). A Non-enzymatic Electrochemical Hydrogen Peroxide Sensor Based on Copper Oxide Nanostructures. *Beilstein J. Nanotechnol., 13,* 424–436. https://doi.org/10.3762/bjnano.13.35